POLITECNICO DI TORINO
Repository ISTITUZIONALE

Assessing Real-Time PPP Performance for PWV Estimation Using Low-Cost GNSS Stations and Multi-Source Correction Products

Original
Assessing Real-Time PPP Performance for PWV Estimation Using Low-Cost GNSS Stations and Multi-Source Correction Products / Bagheri, M., Dabove, P.. - (2026), pp. 745-752. (XXV ISPRS Congress 2026 "From Imagery to Understanding Toronto (Can) 4 -11 July 2026) [10.5194/isprs-archives-XLIX-B3-2026-745-2026].

Availability:
This version is available at: 11583/3014068 since: 2026-08-06T14:23:54Z

Publisher:
Copernicus Publications

Published
DOI:10.5194/isprs-archives-XLIX-B3-2026-745-2026

Terms of use:

This article is made available under terms and conditions as specified in the corresponding bibliographic description in the repository

Publisher copyright

(Article begins on next page)

02 November 2026

Assessing Real-Time PPP Performance for PWV Estimation Using Low-Cost GNSS Stations and Multi-Source Correction Products

Milad Bagheri[1], Paolo Dabove[1]

[1] Dept. of Environment, Land, and Infrastructure Engineering (DIATI), Politecnico di Torino-
(milad.bagheri,paolo.dabove)@polito.it

Keywords: Precise Point Positioning (PPP), Precipitable Water Vapor (PWV),Low-Cost GNSS, GNSS meteorology, Zenith Tropospheric Delays(ZTD), Galileo High Accuracy Service (HAS).

Abstract

Monitoring atmospheric water vapour is essential for weather forecasting and climate studies. GNSS networks can retrieve Precipitable Water Vapour (PWV) continuously at each station location, but the accuracy depends on the quality of the satellite orbit and clock corrections used in the processing. This study evaluates PWV retrieval from 478 stations of the French Centipede low-cost GNSS network using four levels of correction products with decreasing latency: GFZ Final (∼2 weeks), Rapid (∼1 day), Ultra-rapid (3–9 hours), and broadcast ephemerides (real-time). Validation against ERA5 reanalysis shows that the Final and Rapid products achieve similar performance (RMSE $\approx$ 2 mm, r^2 = 0.84), confirming that near-real-time processing introduces no significant accuracy loss. Ultra-rapid products remain usable (RMSE = 3.4 mm), while broadcast ephemerides show larger errors (RMSE = 5.8 mm) but still capture the spatial moisture pattern. In addition, a real-time experiment using the freely available Galileo High Accuracy Service (HAS) demonstrates that stable tropospheric estimates (ZTD $\pm$ 1.4 mm, PWV $\pm$ 0.2 mm) can be obtained in real time, even before the positioning solution has fully converged. These results suggest that combining the spatial density of low-cost networks with real-time HAS corrections could enable high-resolution PWV monitoring that is not achievable with existing systems.

1. Introduction

Atmospheric water vapour is the most abundant greenhouse gas and the primary driver of latent heat transport in the Earth's climate system. Despite constituting less than 4% of the atmosphere by mass, it governs the formation of clouds and precipitation, modulates the planetary energy budget, and amplifies the response to anthropogenic forcing through the well-documented water vapour feedback (Held and Soden, 2000, Trenberth et al., 2005). Precipitable Water Vapour (PWV)—the vertically integrated column of atmospheric water vapour—is therefore a fundamental quantity for Numerical Weather Prediction (NWP), where its accurate initialisation can significantly improve short-range precipitation forecasts (Guerova et al., 2016). In climate monitoring, long-term PWV records are essential for detecting trends in the hydrological cycle and for validating the moisture fields of reanalysis products (Ning et al., 2016). However, conventional observing systems—radiosondes and ground-based radiometers—suffer from limited spatial density, high operational cost, and, in the case of radiosondes, coarse temporal sampling. These constraints leave substantial observational gaps, particularly over data-sparse regions and during rapidly evolving weather events, motivating the search for complementary, cost-effective PWV monitoring techniques.

Global Navigation Satellite System (GNSS) meteorology has emerged as one of the most effective approaches to filling this gap. The technique exploits the delay experienced by GNSS signals as they traverse the neutral atmosphere: the Zenith Tropospheric Delay (ZTD), estimated as a by-product of precise positioning, can be decomposed into a hydrostatic component (ZHD)—accurately modelled from surface pressure—and a wet component (ZWD), which is then converted to PWV through a well-established mapping that depends on the atmospheric mean temperature (Bevis et al., 1992). Since the early demonstrations by Bevis et al. (Bevis et al., 1992), GNSS-derived PWV has been extensively validated against radiosondes, radiometers, and reanalysis products, demonstrating millimetre-level accuracy under a wide range of conditions (Tregoning et al., 1998, Van Malderen et al., 2020). Today, several national and European programmes routinely assimilate GNSS-derived ZTD into operational NWP models, confirming the maturity of the technique (Poli et al., 2007, Guerova et al., 2016). The standard GNSS processing strategy for tropospheric estimation is Precise Point Positioning (PPP), which uses precise satellite orbit and clock products together with un-differenced dual-frequency observations to achieve millimetre-level positioning accuracy and ZTD precision without requiring a reference network (Li et al., 2023). The quality of the orbit and clock products ingested by PPP directly conditions the accuracy of the estimated ZTD and, consequently, of the derived PWV. The International GNSS Service (IGS) coordinates a global network of Analysis Centres (ACs)—including the German Research Centre for Geosciences (GFZ, `https://gnss.gfz.de/products`), the Center for Orbit Determination in Europe (CODE), the Jet Propulsion Laboratory (JPL), and the European Space Agency (ESA)—each of which generates its own suite of orbit and clock products (Johnston et al., 2017). These products follow a common hierarchy with decreasing latency and accuracy: Final products (∼2 weeks latency, highest quality), Rapid products (∼17 hours), and Ultra-rapid products (3–9 hours for the observed half, with 24-hour orbit predictions for real-time use). In addition, broadcast ephemerides (BRDC), transmitted by the satellites themselves, are available instantaneously but carry orbit errors of the order of metres. In the present study, the GFZ multi-GNSS products are adopted, as they provide consistent GPS and Galileo orbit and clock solutions across all product tiers (Männel et al., 2020a, Männel et al., 2020b, Männel et al., 2020c). Several studies have quantified the impact of product quality on ZTD

estimation using geodetic-grade receivers, generally concluding that Final and Rapid products yield equivalent tropospheric performance, whereas Ultra-rapid and BRDC solutions exhibit increased noise and systematic biases (Li et al., 2014, Kazmierski et al., 2018, Yao et al., 2024). However, most of these assessments have been conducted on small sets of geodetic stations, and a systematic evaluation over a dense, spatially extensive network, particularly one composed of low-cost receivers, remains lacking. This gap is significant because the stochastic characteristics and multipath behaviour of low-cost hardware may interact with product errors in ways that are not directly transferable from geodetic-grade benchmarks.

The Centipede RTK network provides a unique opportunity to address this gap. Centipede is a community-driven, open-source network of low-cost dual-frequency GNSS permanent stations deployed across the world, originated from France (`https://centipede.fr/`). With approximately 700 stations as of early 2026, the network offers an unprecedented spatial density of low-cost receivers, most of which are based on u-blox ZED-F9P modules coupled with low-cost antennas. The homogeneity of the hardware and the open availability of RINEX observations, archived by the RENAG data centre (`https://renag.resif.fr/pub/centipede_1s/`), make Centipede an ideal testbed for evaluating the meteorological potential of low-cost GNSS infrastructure at a national scale. Several studies have demonstrated that individual low-cost receivers can yield ZTD estimates comparable to geodetic-grade systems under controlled conditions (Dabove and Bagheri, 2024, Stepniak et al., 2022, Krietemeyer et al., 2020), and recent work has extended this capability to dense network deployments: Bosser et al. (Bosser et al., 2024) performed the first comprehensive evaluation of tropospheric products from the Centipede network, processing 331 stations over the full year 2023 and reporting ZTD agreement with conventional stations at the 7.4 mm RMS level. However, while these studies confirm the tropospheric quality attainable from low-cost hardware, none has yet investigated how the choice of orbit and clock products, from final to broadcast, affects the accuracy and reliability of PWV estimates derived from such networks.

In parallel with the densification of ground infrastructure, the availability of real-time GNSS correction products has grown substantially, opening the door to near-real-time tropospheric monitoring. Among these, the Galileo High Accuracy Service (HAS) represents a paradigm shift: it is the first global, free-of-charge, high-accuracy positioning service broadcast directly via the Galileo E6-B signal and disseminated through the Galileo constellation itself (European Union, 2023b, Fernandez-Hernandez et al., 2022). HAS provides State Space Representation (SSR) corrections for satellite orbits, clocks, and biases for both Galileo and GPS, enabling real-time PPP with a target accuracy of 20 cm horizontally and 40 cm vertically (European Union, 2023b). While an expanding body of literature has characterised HAS positioning performance (Naciri et al., 2023, Jia et al., 2024, Angrisano et al., 2024), the exploitation of HAS-driven PPP for real-time ZTD and PWV retrieval has received comparatively little attention. This is particularly relevant because ZTD estimates can reach meteorologically useful accuracy even before full positional convergence, owing to the quality of a priori tropospheric models and the integrated nature of the tropospheric parameter over all visible satellites.

Against this background, the present study addresses the above-mentioned gaps through a twofold investigation. First, we evaluate the impact of orbit and clock product quality on PPP-derived PWV over the Centipede network, processing approximately 478 stations across metropolitan France with four product tiers—GFZ Final, GFZ Rapid, GFZ Ultra-rapid, and broadcast ephemerides—thereby providing the first large-scale, product-stratified PWV quality assessment based on low-cost GNSS infrastructure. The resulting PWV fields are validated against ERA5 reanalysis Total Column Water Vapour (TCWV), offering a spatially consistent benchmark that enables a rigorous evaluation of the atmospheric information content retrievable from each product tier. Second, in order to evaluate the potential of the Galileo High Accuracy Service for real-time tropospheric monitoring, we conduct a dedicated real-time PPP experiment using HAS SSR corrections, assessing not only positioning accuracy and convergence behaviour under cold-start and warm-start conditions, but also the stability and quality of the estimated ZTD and PWV.

The remainder of this paper is organised as follows. Section 2 describes the GNSS data, correction products, PPP processing strategy, ZTD-to-PWV conversion, and the validation framework for both the multi-product and HAS experiments. Section 3 presents the results and discussion, covering the multi-product PWV assessment over the Centipede network, the Galileo HAS real-time experiment, and the implications for low-cost GNSS tropospheric monitoring. Finally, Section 4 summarises the main conclusions.

2. DATA AND METHODOLOGY

2.1 GNSS Data and Correction Products

The GNSS observations used in this study were collected from the Centipede RTK network(`https://map.centipede-rtk.org/`) for a week in January 2025, a representative winter week over metropolitan France. A total of 478 dual-frequency stations were selected, all equipped with low-cost receivers and antennas tracking multi-constellation signals at a 30 seconds sampling interval. The observations were downloaded in RINEX 3.x format from the RENAG archive (`https://renag.resif.fr/pub/centipede_1s/`).

Four orbit and clock product types were used (Table 1) to process the same set of observations, in order to isolate the effect of product quality on the derived tropospheric and PWV estimates:

Product	Latency
GFZ Final	∼2 weeks
GFZ Rapid	∼1 day
GFZ Ultra-rapid	3–9 hours
Broadcast (BRDC)	Real-time

Table 1. Orbit and clock products used in this study.

All GFZ products were obtained from the GFZ Data Services (`https://gnss.gfz.de/products`).

2.2 PPP Processing

All observations were processed using RTKLIB demo5 b34h, a version of RTKLIB optimized for low-cost GNSS receivers (`https://github.com/rinex20/RTKLIB-demo5`) in static PPP mode with the ionosphere-free linear combination of dual-frequency GPS and Galileo observations. The tropospheric

delay was estimated as a random-walk process comprising the Zenith Tropospheric Delay (ZTD) together with horizontal gradients. The main processing parameters are summarised in Table 2.

Parameter	Setting
Software	RTKLIB demo5 b34h
Positioning mode	PPP-static
Constellations	GPS + Galileo
Frequencies	L1+L2 (ionosphere-free LC)
Filter	Combined
Elevation mask	10°
Troposphere model	ZTD + gradients estimated
ZTD process noise	10^{-4} m/$\sqrt{\text{s}}$
Code/phase noise ratio	300
Ambiguity resolution	Float

Table 2. PPP processing configuration in RTKLIB.

The entire processing chain—from the automated download of RINEX observations and orbit/clock products, through PPP computation with RTKLIB, to the extraction of ZTD and conversion to PWV—was implemented in a Python-based pipeline developed by the authors, ensuring full reproducibility across all four product configurations.

2.3 ZTD Decomposition and PWV Conversion

The ZTD estimated by PPP was decomposed into its hydrostatic and wet components:

$$\text{ZTD} = \text{ZHD} + \text{ZWD} \tag{1}$$

where ZHD is the Zenith Hydrostatic Delay and ZWD is the Zenith Wet Delay. The ZHD was computed using the Saastamoinen model (Saastamoinen, 1972):

$$\text{ZHD} = \frac{0.0022767\,P}{1 - 0.00266\cos(2\varphi) - 0.00028\,h} \tag{2}$$

where P is the surface pressure (hPa), φ is the station latitude, and h is the ellipsoidal height (km). The pressure, temperature, and water vapour pressure required for the computation were provided by the Global Pressure and Temperature 3 (GPT3) model (Landskron and Böhm, 2018), which delivers meteorological parameters at any location and epoch through bilinear interpolation of a $1^\circ \times 1^\circ$ global grid combined with annual and semi-annual harmonic functions. The GPT3 model also provides the weighted mean temperature T_m of the atmosphere, which is needed for the PWV conversion. The ZWD was then obtained by subtracting the modelled ZHD from the PPP-estimated ZTD:

$$\text{ZWD} = \text{ZTD} - \text{ZHD} \tag{3}$$

The conversion from ZWD to PWV follows the formulation of Bevis et al. (Bevis et al., 1992):

$$\text{PWV} = \frac{\text{ZWD}}{Q} \tag{4}$$

where Q is a dimensionless conversion factor defined as:

$$Q = 10^{-6}\,\rho_w\,R_v\left(k_2' + \frac{k_3}{T_m}\right) \tag{5}$$

where $\rho_w = 1000\ \text{kg m}^{-3}$ the density of liquid water, $R_v = 461.5\ \text{J kg}^{-1}\,\text{K}^{-1}$ the specific gas constant for water vapour, $k_2' = 0.221\ \text{K Pa}^{-1}$ and $k_3 = 3776\ \text{K}^2\,\text{Pa}^{-1}$ the refractivity constants, and T_m the weighted mean temperature (K) provided by GPT3.

2.4 Validation Against ERA5 Reanalysis

The GNSS-derived PWV fields were validated against the Total Column Water Vapour (TCWV) product from the ERA5 reanalysis (Hersbach et al., 2020), produced by the European Centre for Medium-Range Weather Forecasts (ECMWF). ERA5 provides hourly estimates of atmospheric variables on a global $0.25^\circ \times 0.25^\circ$ grid, assimilating a wide range of satellite and in-situ observations into a state-of-the-art numerical weather model. The TCWV field, expressed in kg m^{-2} (numerically equivalent to mm of PWV), was downloaded via the Copernicus Climate Data Store (CDS) API for the domain.

For each GNSS station, the ERA5 TCWV value was obtained by bilinear interpolation from the four surrounding grid points. The comparison was performed at multiple epochs throughout the day, computing across all valid stations for each product tier. This station-dense, product-stratified comparison methodology enables a spatially resolved assessment of the PWV quality achievable from low-cost GNSS infrastructure under different orbit/clock scenarios.

2.5 Galileo High Accuracy Service (HAS) Correction

In addition to the post-processed GFZ orbit and clock products described above, the Galileo High Accuracy Service (HAS) offers a fundamentally different approach to PPP corrections. Unlike GFZ products, which are derived from post-processing or near-real-time estimation and distributed with latencies ranging from hours to weeks, HAS provides State Space Representation (SSR) corrections, comprising satellite orbit corrections, clock corrections, and code biases for both GPS and Galileo, generated in real time by the High Accuracy Data Generator (HADG) and disseminated with a nominal update rate of 10 seconds (European Union, 2023a). These corrections are delivered through two complementary channels: directly via the Galileo E6-B signal component, and over the internet through the Internet Data Distribution (IDD) interface, which employs the NTRIP protocol (European Union, 2023a). This dual dissemination strategy, combined with the free-of-charge access and the absence of reliance on external processing centres, makes HAS a particularly attractive option for real-time PPP applications. In the present study, the HAS corrections were received via the IDD channel and applied in real time using the BKG Ntrip Client (BNC) version 2.13.4 (`https://igs.bkg.bund.de/ntrip/bnc`), configured in PPP mode. The experiment was carried out on several EPN stations. Since HAS currently provides corrections only for GPS and Galileo, GLONASS and BeiDou constellations were disabled to avoid degrading the solution with uncorrected observations. The main processing parameters are summarised in Table 3.

The ZTD estimated by BNC was then processed through the same Python-based pipeline developed by the authors and described in Section 2.3, applying the Saastamoinen model with

Parameter	Setting
Software	BNC v2.13.4
Mode	Real-time PPP
SSR source	Galileo HAS (IDD)
Constellations	GPS + Galileo
Frequencies	Dual-frequency (ionosphere-free)
Elevation mask	7°
Coordinate process noise	0.1 m/$\sqrt{s}$
Phase residual threshold	0.03 m
Code residual threshold	3.0 m

Table 3. BNC real-time PPP configuration for the HAS experiment.

GPT3-derived pressure for ZHD computation and the Bevis conversion factor for the ZWD-to-PWV transformation. This ensures full consistency between the tropospheric products derived from the post-processing and the real-time experiments. The positioning performance was evaluated against the known station coordinates, while the PWV stability were assessed across the processing sessions.

3. Result and Discussion

This section presents the results of the multi-product PWV assessment over the Centipede network. Although one full week of January 2025 was processed, the results shown here focus on 15 January 2025 as a representative winter day. The analysis proceeds from the spatial PWV fields, through temporal variability at selected stations, to a systematic validation against ERA5 reanalysis at both network and station level.

Figure 1 shows the spatial distribution of daily mean PWV across metropolitan France as derived from the four product tiers. The Final solution (mean PWV = 13.0 mm) reveals a coherent moisture pattern characteristic of a winter day, with higher PWV values (18–21 mm) in northern France, where maritime air masses dominate, and lower values (5–8 mm) over the elevated terrain of the Alps. The Rapid solution (13.1 mm) is virtually indistinguishable from the Final, reproducing the same spatial gradients with no visible difference, which confirms that the one-day latency reduction carries negligible impact on tropospheric estimation. The Ultra-rapid solution (12.6 mm) preserves the overall spatial structure but exhibits a slight negative offset relative to the Final, with some stations, particularly at mid-elevations, showing locally degraded estimates. The BRDC solution (14.3 mm) stands in clear contrast. These differences reflect the degraded orbit and clock accuracy of broadcast ephemerides, which propagates directly into the ZTD estimates and, consequently, into the derived PWV.

Moreover, to examine the temporal behaviour of the estimates, six stations spanning a wide range of elevations (8 to 2276 m a.s.l.) were selected. Figure 2 shows the hourly mean PWV time series for each product type. The Final and Rapid solutions produce nearly identical, smooth time series at all stations, with PWV values generally following an elevation gradient as expected from the exponential decrease of water vapour with altitude. The Ultra-rapid solution preserves the overall elevation-dependent structure but introduces significant outlier spikes at several epochs, most notably at mid-elevation stations such as A742 (301 m), where the PWV intermittently jumps to values comparable to the lowest-lying station, indicating that the predicted orbit half occasionally introduces large errors that

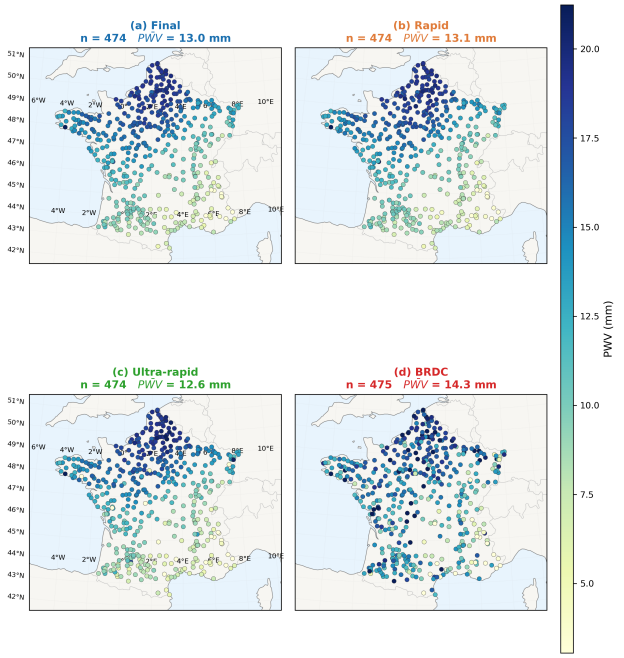


Figure 1. Spatial distribution of daily mean PWV on a representative day (15.01.2025) using different GFZ products.

propagate into the tropospheric estimates. The BRDC solution shows a different type of degradation: instead of random spikes, the PWV values at all stations tend to converge towards similar levels, reducing the natural spread between low- and high-altitude stations. In particular, stations at high elevations (A523, A502) show PWV values much higher than expected, and the well-defined elevation gradient seen in the Final and Rapid solutions is largely lost. This behaviour can be explained by the large orbit errors in broadcast ephemerides, which are partly absorbed by the ZTD estimate during PPP processing, with a stronger effect at higher stations where it is more difficult to separate the tropospheric delay from the vertical coordinate.

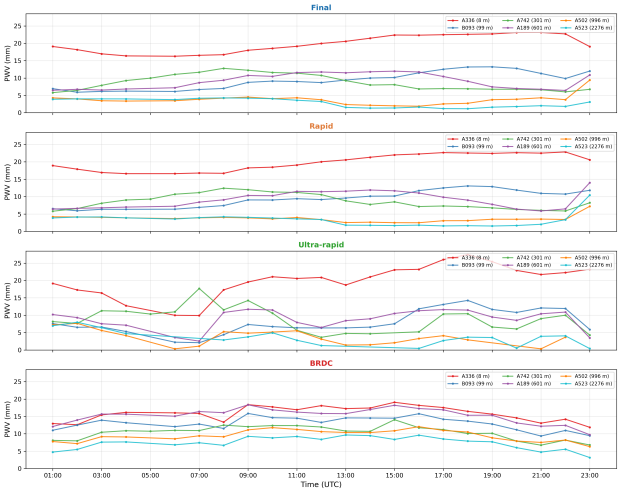


Figure 2. Hourly mean PWV time series for six representative stations at different elevations, obtained by using different product type.

The GNSS-derived PWV were validated against ERA5 TCWV at different hours. Figure 3 presents the scatter plots and spa-

tial bias maps, while Figure 4 shows the corresponding residual histograms. Table 4 summarises the validation statistics.

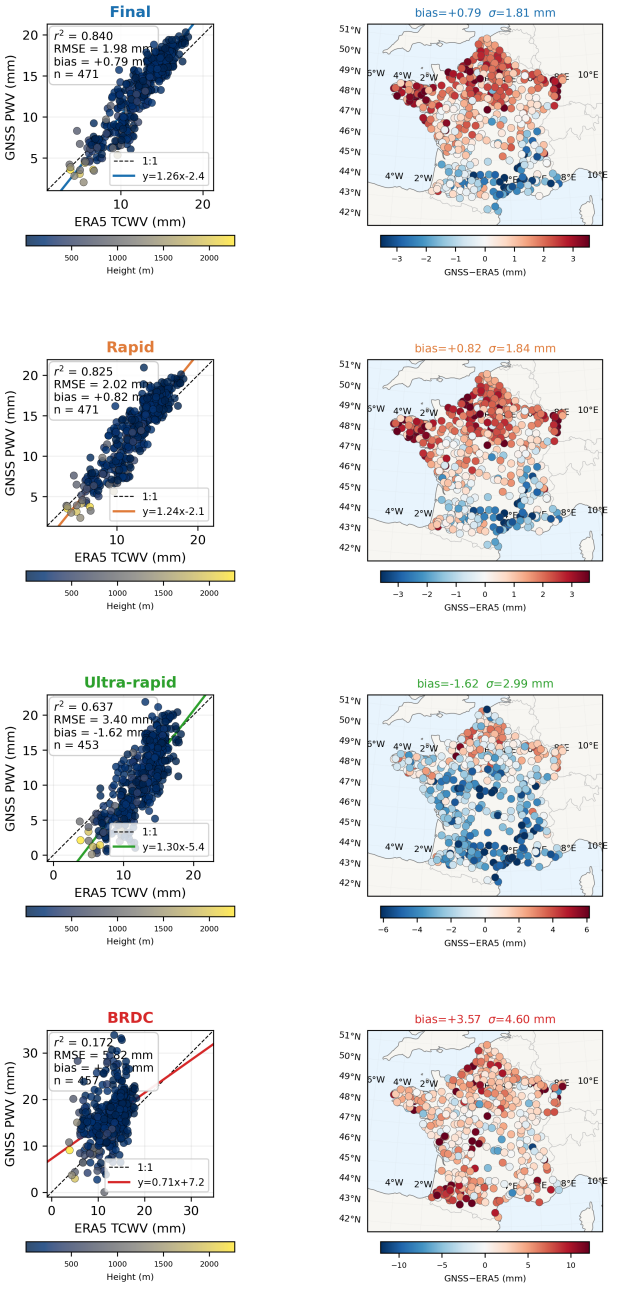


Figure 3. GNSS PWV versus ERA5 TCWV at 12:00 UTC. Each row: scatter plot colour-coded by height (left) and spatial bias map (right). From top to bottom: Final, Rapid, Ultra-rapid, BRDC.

The Final and Rapid products show excellent agreement with ERA5, with RMSE values of 1.98 and 2.02 mm, standard deviations of 1.81 and 1.84 mm, and correlation coefficients (r^2) of 0.84 and 0.83, respectively. The regression slopes of 1.26 and 1.24 indicate that the GNSS-derived PWV tends to overestimate ERA5 at higher moisture levels while slightly underestimating at very low values, as reflected by the negative intercepts of the regression lines. This behaviour may partly result from the spatial smoothing inherent in the ERA5 grid ($0.25°$), which tends to dampen extreme values, as well as from residual errors in the GPT3-derived meteorological parameters used in the ZWD-to-PWV conversion. The bias maps reveal a weak positive bias across most of the country ($+0.79$ and $+0.82$ mm), with no dominant spatial pattern. The Ultra-rapid solution degrades noticeably, with an RMSE of 3.40 mm, a negative bias of -1.62 mm, and a broader residual distribution ($\sigma = 2.99$ mm). The BRDC solution performs substantially worse. The regression slope of 0.71 indicates a compressed dynamic range, meaning the BRDC-derived PWV fails to capture the full amplitude of the atmospheric moisture field. The same degradation pattern is also evident in the residual histograms (Figure 4), where the distributions progressively widen from Final to BRDC.

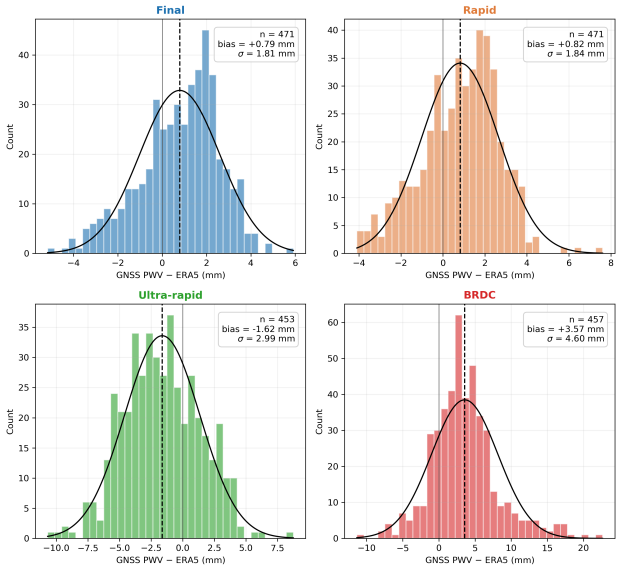


Figure 4. Residual histograms of GNSS PWV − ERA5 TCWV at 12:00 UTC for each product tier.

Product	Bias	RMSE	Std	r^2
Final	+0.79	1.98	1.81	0.84
Rapid	+0.82	2.02	1.84	0.83
Ultra-rapid	−1.62	3.40	2.99	0.64
BRDC	+3.57	5.82	4.60	0.17

Table 4. Summarized ERA5 validation statistics at 12:00 UTC.

To further investigate the structure of the GNSS−ERA5 residuals, Figure 5 presents the PWV difference as a function of station altitude. All four product types exhibit a negative gradient ranging from -1.4 to -2.0 mm/km. For the Final and Rapid products, the residuals are positive at low altitudes and decrease towards zero or slightly negative values at higher elevations; for Ultra-rapid, the residuals are negative at all altitudes but follow the same downward trend; for BRDC, a strong positive offset is present at all elevations with a similar gradient. This altitude-dependent behaviour is largely attributable to the mismatch between the actual station height and the effective altitude of the ERA5 grid cell: at low-lying stations, particularly in valleys and coastal areas, the ERA5 orography overestimates the true terrain height, resulting in a drier atmospheric column in the reanalysis compared to what the GNSS receiver actually senses. Importantly, the gradient is consistent across all four product types, which means it is not caused by the quality of the orbit and clock products but rather by the inherent difference between the point-wise GNSS measurement and the grid-averaged ERA5 representation of the atmosphere.

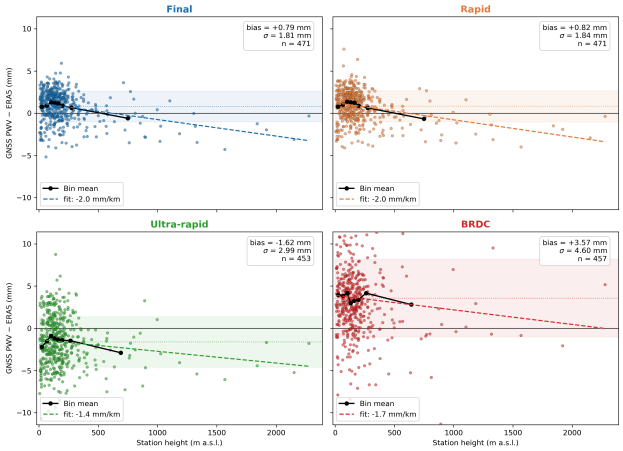


Figure 5. GNSS PWV − ERA5 TCWV as a function of station altitude.

To complement the network-wide analysis, six individual stations spanning elevations from 8 to 2276 m a.s.l. were selected for a detailed hourly comparison against ERA5. Table 5 reports the RMSE for each product tier, and Figure 6 shows the corresponding hourly difference time series. The product-quality ranking observed at network level is confirmed at station level: Final and Rapid achieve sub-3 mm RMSE at all stations, Ultra-rapid degrades to 2–4 mm, and BRDC reaches up to 8 mm at mid-altitude sites such as A189 (601 m). The hourly time series further reveal that Final and Rapid residuals generally remain within ±2–3 mm, with the best agreement at mid-elevation inland stations, while Ultra-rapid exhibits occasional excursions exceeding 5 mm and BRDC shows a predominantly positive offset with the largest deviations (up to 10 mm) at elevated sites.

Station	**h (m)**	Final	Rapid	Ultra	BRDC
A336	8	2.80	2.82	3.70	3.62
B093	99	1.42	1.44	2.39	4.95
A742	301	1.11	1.34	2.61	3.06
A189	601	1.98	2.42	3.06	8.02
A502	996	1.87	1.17	2.00	6.99
A523	2276	1.22	1.85	2.27	5.46

Table 5. Station-level RMSE (mm) against ERA5 on 15 January 2025.

The preceding results established that GFZ Final and Rapid products yield PWV estimates in close agreement with ERA5 reanalysis (RMSE = 1.98 mm, $R = 0.92$ for Final), while Ultra-rapid and broadcast orbits exhibit progressively larger errors. A natural question is whether freely available real-time corrections can bridge the gap between post-processed accuracy and operational latency. To explore this, we conducted a proof-of-concept experiment using the Galileo High Accuracy Service (HAS).

Several test runs were conducted at different stations using HAS corrections received via the IDD channel and processed in real time with BNC. Table 6 summarises the cold-start convergence behaviour for a representative station by reporting the 3D position error at selected epochs after filter initialisation. The solution converges from approximately 9 m (3D) at the first epoch to sub-2 m after 90 minutes and reaches sub-metre accuracy after about 130 minutes.

Figure 7 presents the East, North, and Up position error

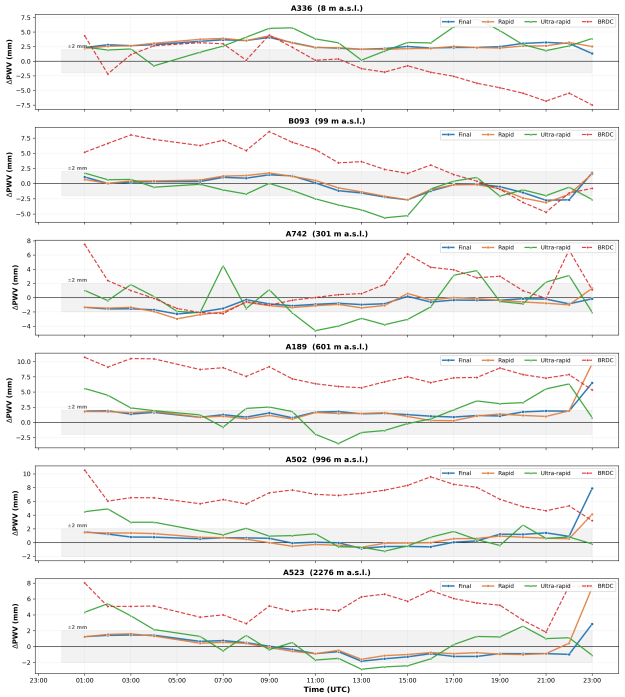


Figure 6. Hourly GNSS PWV − ERA5 TCWV difference time series for six representative stations. Grey shading indicates the ±2 mm band.

Min	**dE (m)**	**dN (m)**	**dU (m)**	**3D (m)**
1	−2.13	+4.05	+7.71	8.96
30	−0.81	+1.22	+4.22	4.47
60	−0.34	+1.27	+4.67	4.85
90	−1.32	+0.67	+0.57	1.58
120	−0.50	−2.60	+0.36	2.67
130	−0.40	−0.09	−0.42	0.58

Table 6. Cold-start convergence of HAS-PPP at the IENG EPN station (Torino, Italy, ∼316 m a.s.l.). Position errors relative to known coordinates of the station.

time series for a representative one-hour window (03:15–04:15 UTC) during a warm-start run. After convergence, the individual components settle to RMS values of 23 cm (East), 36 cm (North), and 34 cm (Up), corresponding to a 3D RMS of 54 cm. The solution remains within the ±0.4 m band for most of the period, although a brief excursion to −2.5 m is visible in the Up component around 04:10 UTC, likely caused by a temporary loss or degradation of the SSR corrections. These positioning results are broadly consistent with the HAS target performance levels reported by Fernandez-Hernandez et al. (Fernandez-Hernandez et al., 2022) and Naciri et al. (Naciri et al., 2023), though the cold-start convergence time in our experiment (approximately 90–130 minutes to sub-metre level) is substantially longer than the nominal 300 s reported in those studies, a difference that may be attributed to the BNC filter configuration.

Figure 8 shows the ZTD, ZWD, and PWV time series derived from the same run. Despite the decimetre-level positioning noise, the estimated ZTD is remarkably stable at 2296.9 ± 1.4 mm over a six-hour window, with the ZHD contribution from the Saastamoinen model fixed at 2254.9 mm. The resulting ZWD of 42.0 ± 1.4 mm and PWV of 6.4 ± 0.2 mm are

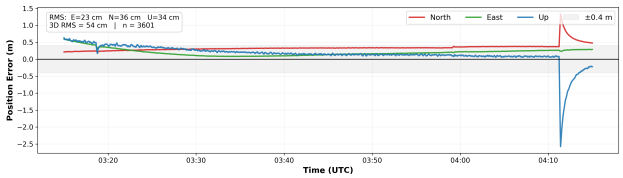


Figure 7. East, North, and Up position error at IENG during a warm-start HAS-PPP run (03:15–04:15 UTC). Grey shading indicates the ±0.4 m band. RMS values are indicated in the legend.

physically consistent with the expected atmospheric conditions at ∼316 m elevation in the Po Valley in early spring. Notably, the ZTD values were consistent across all processing runs to within 0.5–1.5 mm, indicating that the tropospheric estimates converge faster and are more robust to the filter initialisation strategy than the station coordinates. This is an encouraging result for real-time tropospheric monitoring, as it suggests that HAS-driven PPP can deliver stable ZTD and PWV estimates even when the positioning solution has not yet fully converged.

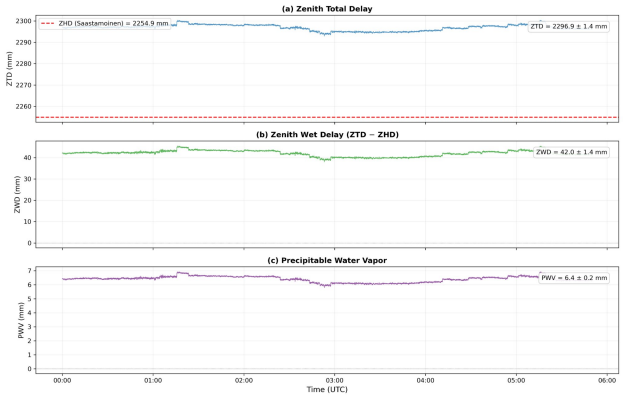


Figure 8. ZTD, ZWD, and PWV time series at IENG from HAS-PPP (warm-start run, 2026-04-03). Red dashed line: ZHD from Saastamoinen model with GPT3.

Although the HAS real-time experiment was conducted exclusively at EUREF permanent stations equipped with geodetic-grade receivers and calibrated antennas, the results confirmed that HAS-driven PPP can deliver stable ZTD estimates (±1.4 mm) and physically plausible PWV values even when the positioning solution is still at the decimetre level. However, HAS corrections have not yet been tested on the Centipede low-cost receivers, where the lack of individual antenna phase centre calibrations is expected to introduce additional biases in both the vertical coordinate and the tropospheric estimates. This limitation is an engineering challenge rather than a fundamental one: as low-cost antenna calibration models become available, there is no reason why HAS corrections could not be applied to dense low-cost networks such as Centipede. Combining the spatial density demonstrated in the first part of this study (∼478 stations over France) with the real-time capability of HAS would open the door to operational, real-time PWV monitoring at a spatial resolution that does not exist today with any current system.

4. Conclusion

This study assessed the feasibility of retrieving precipitable water vapour from the Centipede low-cost GNSS network using multi-product PPP, and explored the potential of Galileo HAS corrections for real-time tropospheric monitoring.

Processing 478 Centipede stations across metropolitan France with four GFZ orbit and clock product tiers showed that Final and Rapid products deliver PWV estimates in close agreement with ERA5 reanalysis, with RMSE values around 2 mm and $r^2 = 0.84$. The two products are virtually interchangeable for tropospheric purposes, meaning that Rapid latency (∼1 day) carries no measurable penalty compared to Final. The Ultra-rapid product remains usable but with reduced precision (RMSE = 3.4 mm), while broadcast ephemerides introduce significant biases (RMSE = 5.8 mm) that limit quantitative use but still capture the overall spatial moisture pattern. An altitude-dependent bias of -1.4 to -2.0 mm/km was found to be consistent across all product types, confirming that it originates from the representativeness mismatch between point-wise GNSS observations and the ERA5 grid rather than from the correction products themselves.

The Galileo HAS real-time experiment demonstrated that SSR corrections delivered via the IDD channel can produce stable ZTD estimates (±1.4 mm) and physically plausible PWV values (6.4 ± 0.2 mm), even when the positioning solution remains at the decimetre level. The tropospheric parameters were found to be more robust to the filter initialisation strategy than the station coordinates, which is an encouraging property for operational deployment.

These two components together suggest a clear pathway: the Centipede network provides the spatial density, while HAS provides the real-time corrections. As low-cost antenna phase centre calibration models become available, combining these two elements could enable real-time, high-density PWV monitoring over France at a resolution that is currently not achievable with any existing system.

5. Acknowledgment

The research activity has been carried out within the SPACE IT UP! project founded by the Italian Space Agency’s Call for ”Space Activities” (topic 15), related to MUR call n°341 of 03/15/2022, for ”Partnerships extended to universities, research centers, companies for the financing of basic research projects” (Prot. CI-2022-DSR-042 of 18 July 2022) financed by Decree of Award of the Italian Space Agency n. 53 of 01/26/2024 - CUP E53C24000300006. “Earth Observation Fund - Financing from the Presidency of the Council of Ministers pursuant to Art. 1, paragraph 254, of law 160/2019. The reference year 2024”.

References

Angrisano, A., Bagheri, M., Cappello, G., Dabove, P., Del Pizzo, S., Gaglione, S., Gioia, C., Portelli, G., Troisi, S., 2024. Analysis of HAS performance in pedestrian navigation with different grade devices. *Proceedings of the 37th International Technical Meeting of the Satellite Division of the Institute of Navigation (ION GNSS+ 2024)*, Baltimore, Maryland, 2123–2135.

Bevis, M., Businger, S., Herring, T. A., Rocken, C., Anthes, R. A., Ware, R. H., 1992. GPS meteorology: Remote sensing of atmospheric water vapor using the Global Positioning System. *J. Geophys. Res. Atmos.*, 97(D14), 15787–15801.

Bosser, P., Ancelin, J., Métois, M., Rolland, L., Vidal, M., 2024. Evaluation of tropospheric estimates from CentipedeRTK, a collaborative network of low-cost GNSS stations. *GPS Solut.*, 28, 158. doi.org/10.1007/s10291-024-01699-3.

Dabove, P., Bagheri, M., 2024. Enhancing atmospheric monitoring capabilities: A comparison of low- and high-cost GNSS networks for tropospheric estimations. *Remote Sens.*, 16(12), 2223. doi.org/10.3390/rs16122223.

European Union, 2023a. Galileo High Accuracy Service – Internet Data Distribution Interface Control Document (HAS IDD ICD), Issue 1.1. European Union Agency for the Space Programme (EUSPA). doi.org/10.2878/607575.

European Union, 2023b. Galileo High Accuracy Service – Service Definition Document (HAS SDD), Issue 1.0. European Union Agency for the Space Programme (EUSPA). gsc-europa.eu.

Fernandez-Hernandez, I., Chamorro-Moreno, A., Cancela-Diaz, S., Calle-Calle, J. D., Zoccarato, P., Blonski, D., Senni, T., de Blas, F. J., Hernández, C., Simón, J., Mozo, A., 2022. Galileo high accuracy service: Initial definition and performance. *GPS Solut.*, 26(3), 65.

Guerova, G., Jones, J., Douša, J., Dick, G., de Haan, S., Pottiaux, E., Bock, O., Pacione, R., Elgered, G., Vedel, H., Bender, M., 2016. Review of the state of the art and future prospects of the ground-based GNSS meteorology in Europe. *Atmos. Meas. Tech.*, 9(11), 5385–5406. doi.org/10.5194/amt-9-5385-2016.

Held, I. M., Soden, B. J., 2000. Water vapor feedback and global warming. *Annu. Rev. Energy Environ.*, 25, 441–475.

Hersbach, H., Bell, B., Berrisford, P., Hirahara, S., Horányi, A., Muñoz-Sabater, J., Nicolas, J., Peubey, C., Radu, R., Schepers, D., Simmons, A., Soci, C., Abdalla, S., Abellan, X., Balsamo, G., Bechtold, P., Biavati, G., Bidlot, J., Bonavita, M., De Chiara, G. et al., 2020. The ERA5 global reanalysis. *Q. J. R. Meteorol. Soc.*, 146(730), 1999–2049.

Jia, Y., Yang, L., Ren, S., Qin, S., Ye, F., Gao, Y., 2024. Initial performance assessment of Galileo High Accuracy Service with software-defined receiver. *GPS Solut.*, 28(1), 2.

Johnston, G., Riddell, A., Hausler, G., 2017. The International GNSS Service. P. J. G. Teunissen, O. Montenbruck (eds), *Springer Handbook of Global Navigation Satellite Systems*, Springer, Cham, 967–982.

Kazmierski, K., Sośnica, K., Hadas, T., 2018. Quality assessment of multi-GNSS orbits and clocks for real-time precise point positioning. *GPS Solut.*, 22(1), 11.

Krietemeyer, A., van der Marel, H., van de Giesen, N., ten Veldhuis, M.-C., 2020. High quality zenith tropospheric delay estimation using a low-cost dual-frequency receiver and relative antenna calibration. *Remote Sens.*, 12(9), 1393. doi.org/10.3390/rs12091393.

Landskron, D., Böhm, J., 2018. VMF3/GPT3: Refined discrete and empirical troposphere mapping functions. *J. Geod.*, 92(4), 349–360. DOI:10.1007/s00190-017-1066-2.

Li, X., Barriot, J.-P., Lou, Y., Zhang, W., Li, P., Shi, C., 2023. Towards millimeter-level accuracy in GNSS-based space geodesy: A review of error budget for GNSS Precise Point Positioning. *Surv. Geophys.*, 44, 1691–1780.

Li, X., Dick, G., Ge, M., Heise, S., Wickert, J., Bender, M., 2014. Real-time GPS sensing of atmospheric water vapor: Precise point positioning with orbit, clock, and phase delay corrections. *Geophys. Res. Lett.*, 41(10), 3615–3621.

Männel, B., Brandt, A., Nischan, T., Brack, A., Sakic, P., Bradke, M., 2020a. GFZ final product series for the International GNSS Service (IGS). GFZ Data Services. doi.org/10.5880/GFZ.1.1.2020.002.

Männel, B., Brandt, A., Nischan, T., Brack, A., Sakic, P., Bradke, M., 2020b. GFZ rapid product series for the IGS. GFZ Data Services. doi.org/10.5880/GFZ.1.1.2020.003.

Männel, B., Brandt, A., Nischan, T., Brack, A., Sakic, P., Bradke, M., 2020c. GFZ ultra-rapid product series for the IGS. GFZ Data Services. doi.org/10.5880/GFZ.1.1.2020.004.

Naciri, N., Yi, D., Bisnath, S., de Blas, F. J., Capua, R., 2023. Assessment of Galileo High Accuracy Service (HAS) test signals and preliminary positioning performance. *GPS Solut.*, 27(2), 73.

Ning, T., Wickert, J., Deng, Z., Heise, S., Dick, G., Vey, S., Schöne, T., 2016. Homogenized time series of the atmospheric water vapor content obtained from the GNSS reprocessed data. *J. Climate*, 29(7), 2443–2456.

Poli, P., Moll, P., Rabier, F., Desroziers, G., Chapnik, B., Berre, L., Healy, S. B., Andersson, E., El Guelai, F.-Z., 2007. Forecast impact studies of zenith total delay data from European near real-time GPS stations in Météo France 4DVAR. *J. Geophys. Res. Atmos.*, 112(D6), D06114.

Saastamoinen, J., 1972. Atmospheric correction for the troposphere and stratosphere in radio ranging of satellites. S. W. Henriksen, A. Mancini, B. H. Chovitz (eds), *The Use of Artificial Satellites for Geodesy*, American Geophysical Union, Washington, D.C., 247–251.

Stepniak, K., Paziewski, J., Kruczyk, M., 2022. Applicability of low-cost GNSS receivers in precise ZTD estimation. *Measurement*, 195, 111350.

Tregoning, P., Boers, R., O’Brien, D., Hendy, M., 1998. Accuracy of absolute precipitable water vapor estimates from GPS observations. *J. Geophys. Res. Atmos.*, 103(D22), 28701–28710.

Trenberth, K. E., Fasullo, J., Smith, L., 2005. Trends and variability in column-integrated atmospheric water vapor. *Climate Dyn.*, 24(7–8), 741–758.

Van Malderen, R., Brenot, H., Tanré, D., Beirle, S., Bock, O., Brogniez, C. and”; Campistron, B., Dabas, A., Delcloo, A., Pazmino, A., 2020. A multi-site intercomparison of integrated water vapour observations for climate change analysis. *Atmos. Meas. Tech.*, 13(5), 2797–2823. doi.org/10.5194/amt-13-2797-2020.

Yao, W., Zhao, Q., Li, L., Wang, C., Shu, B., 2024. Multi-GNSS real-time tropospheric delay retrieval based on multi-system SSR products. *Ann. Geophys.*, 42, 455–472. doi.org/10.5194/angeo-42-455-2024.